PREDICTIONS OF WALL-PRESSURE FLUCTUATION IN SEPARATED COMPLEX FLOWS WITH IMPROVED LES AND QUASI-DNS

Masahide Inagaki, Nariaki Horinouchi
Digital Engineering Lab.,
Toyota Central Research & Development Laboratories, Inc.
Nagakute, Aichi 480-1192, Japan
masa@cfd.tytlabs.co.jp, hor@cfd.tytlabs.co.jp

Ken-ichi Ichinose
Vehicle Engineering Div.,
Toyota Motor Corporation
Toyota-cho, Toyota, Aichi 471-8571, Japan
ichinose@giga.tec.toyota.co.jp

Yasutaka Nagano
Department of Mechanical Engineering,
Nagoya Institute of Technology
Gokiso-cho, Showa-ku, Nagoya, 466-8555, Japan
nagano@heat.mech.nitech.ac.jp

ABSTRACT

To seek a practical methodology for predicting the wall-pressure fluctuation associated with the aerodynamic noise radiated from the flow around bluff bodies at low Mach number, we conducted some calculations of the flow around a circular cylinder, which includes some LES using the Smagorinsky model, the dynamic Smagorinsky model and a new mixed-time-scale SGS model (Inagaki *et al.* 2002a), as well as Quasi-DNS. The comparative results are examined, revealing that LES with the new mixed-time-scale SGS model is most accurate in predicting not only the mean flow field and turbulent intensities but also the wall-pressure fluctuation, and is more stable than the dynamic model. It is also confirmed that Quasi-DNS is less accurate than LES using any SGS model, and that LES using QUICK scheme for the convection term gives similar results to those obtained by Quasi-DNS. Furthermore, calculations of the flow around a simplified front-pillar model of an automobile are also performed. The corresponding experiment shows that the wall-pressure fluctuation has a wide-range spectrum. The results of LES using the new SGS model show better agreement with the experimental data in a high-frequency range than those of quasi-DNS. Thus, it is concluded that LES with the mixed-time-scale SGS model is an effective method for predicting certain kinds of wall-pressure fluctuations.

INTRODUCTION

Various kinds of aerodynamic noise problems are associated with automobiles, e.g., wind noise from the front-pillar and rear-view mirror, whistling from the front-grill, an Aeolian tone from the pole-antenna, fan noise from the air-conditioning blower and engine cooling fan, windthrob noise within the cabin with the sun-roof or window open. These noises are categorized into three types. First, those with a strong peak spectrum such as whistling or the Aeolian tone. Second, those with wide-range spectra such as wind and fan noises. Third, resonance noises caused by fluid-resonant oscillation such as windthrob noise.

The third is different from the other two because resonance strongly influences the flow field. In predicting such a flow, it is essential to take account of the weak compressibility effect of the flow at low Mach number. Inagaki *et al.* (2002b) have developed a new numerical method suited for capturing such compressibility effects. In this study, a new equation set was derived under the assumption that the compressibility effect is weak, and a pressure-based method was applied to alleviate the stiffness problem that arises in solving the usual compressible flow equations under low Mach number. Employing this numerical method, the effect of resonance at low Mach number can be directly simulated with almost the same computational effort as for the incompressible flow calculation. Its validity was confirmed in computations of the flows over a three-dimensional open cavity, where the frequency of the pressure fluctuations is locked in at the Helmholtz resonant frequency as in the experiment, and the agreement both in the frequency and in the pressure fluctuation level is quite satisfactory.

On the other hand, the other two types of aerodynamic noises can be predicted by performing incompressible simulations and using Lighthill-Curle's theory (Curle 1955). According to this theory, in general, the far-field sound radiating from the flow around bluff bodies at low Mach number can be described as follows:

$$p_a = \frac{1}{4\pi a}\frac{x_i}{r^2}\frac{\partial}{\partial t}\int_S n_i p\left(y, t-\frac{r}{a}\right) dS, \qquad (1)$$

where p_a denotes the radiated sound pressure, a the speed of sound, x_i the location of the observation point, S the surface of the body, r the distance between the body surface point and the observation point, n_i the outward unit vector normal to the surface, p the static pressure, and y the coordinate at the body surface point. As a consequence, the far-field radiated sound pressure can be calculated from the fluctuating surface pressure obtained by the unsteady flow simulation. Accordingly, it is most important to predict the

wall-pressure fluctuations with high accuracy when predicting aerodynamic noise.

As for the calculation method of unsteady flows, DNS is most desirable for such calculations due to its high accuracy. However, it is impossible to employ DNS in the engineering calculation because of its high cost. Alternative means are LES and Quasi-DNS (Q-DNS). LES has become applicable to engineering predictions thanks to recent advances in computers and sub-grid-scale (SGS) modeling, and the prediction of aerodynamic noise is considered to be one of the effective applications of LES. The dynamic Smagorinsky model proposed by Germano *et al.* (1991) has enhanced the applicability of LES to complex flows. This model has been proved able to overcomes the following defects of the conventional Smagorinsky model: (1) The model must be supplemented with a wall-damping function of the van Driest type; (2) The model parameter needs to be adjusted according to the type of flow field; (3) The SGS effect does not disappear in the laminar flow region.

In spite of the remarkable success of the dynamic Smagorinsky model, however, some problems have occurred in its practical use. First, the SGS eddy viscosity obtained by using the dynamic procedure is not guaranteed to be positive, which leads to numerical instability and increased computational cost. Inagaki *et al.* (2002a) have experienced such an instability in their calculation of a backward-facing step flow even though both the averaging in a spanwise direction and the clipping, which sets the negative SGS eddy viscosity to zero, were performed. Second, in engineering applications, the computational accuracy is lower than the Smagorinsky model with the model parameter optimized for the relevant flow field. This may be caused by artificial approaches used in the calculation of the model parameter (e.g., clipping, volume average). In addition, the difference of the filtering procedure is considered to be another significant reason. Filtering is ordinarily done in the streamwise and spanwise directions, and not in the wall-normal direction. However, it is difficult to define the wall-normal direction in complex geometries. Thus, in engineering applications, an all-directional filtering procedure is usually adopted. Inagaki *et al.* (2002a) have showed it in their calculation of a backward-facing step flow that the value of the model parameter obtained using the all-directional filtering differs markedly from that with ordinal two-directional filtering. This discrepancy probably leads to the diminished accuracy of the dynamic Smagorinsky model in engineering applications.

To improve the accuracy and computational stability of practical LES, Inagaki *et al.* (2002a) have proposed a new SGS model constructed with the concept of mixed time scale, which makes it possible to use consistent model-parameters and to dispense with a wall-damping function of the van Driest type. The model performance was tested in plane channel flows, a backward-facing step flow and the three-dimensional complex flow around an Ahmed's bluff body. The results showed that the use of fixed model-parameters provides computational stability, and that the accuracy of the proposed model is as good as that of the Smagorinsky model with the model parameter optimized for the relevant flow field, and is even superior to the dynamic Smagorinsky model using the all-directional filtering procedure. Since the present model is easily applied to flows with complex geometries, it promises to be widely accepted as a refined SGS model suited to practical engineering-relevant LES.

On the other hand, Q-DNS, which employs a third-order upwind scheme for the convective term and no turbulence model, continues to be widely used in engineering applications. Some studies (e.g., Horinouchi *et al.* 1995) have shown that Q-DNS has the capability of predicting the averaged drag coefficient of bluff bodies with relatively high accuracy. However, the artificial viscosity introduced by a third-order upwind scheme probably contaminates the turbulent components of the flow field, which poses a serious problem at least in predicting aerodynamic noises. It should be noted that some LES calculations (e.g., Neto *et al.* 1993, Jordan 2002) have been performed together with a third-order upwind scheme for the convective term, in which the same problem presumably takes place as that in Q-DNS.

Thus, our aim is to seek a practical methodology for predicting the wall-pressure fluctuation associated with aerodynamic noise. First, to examine the validity of the mixed-time-scale SGS model in outer flows, we apply it to the flow around a circular cylinder, and its computational stability and accuracy are compared with both the conventional Smagorinsky and dynamic Smagorinsky models. Next, to elucidate the effect of artificial viscosity, the computational results of LES, employing a second-order central difference scheme, are compared with those of Q-DNS. In addition, LES employing the upwind scheme for the convective term is also investigated. Furthermore, we apply the present LES and Q-DNS methods to the flow around a simplified front-pillar model of an automobile. The spectra of the wall-pressure fluctuations broaden over a wide range in contrast to those of the circular cylinder. The capability of each method to predict pressure fluctuations with wide-range spectra is comparatively examined using three kinds of grid resolutions.

GOVERNING EQUATIONS

The basic equations are the filtered Navier-Stokes and continuity equations for an incompressible fluid:

$$\frac{\partial \overline{u}_j}{\partial x_j} = 0, \tag{2}$$

$$\frac{\partial \overline{u}_i}{\partial t} + \frac{\partial \overline{u}_j \overline{u}_i}{\partial x_j} + \frac{\partial \tau_{ij}}{\partial x_j} = -\frac{1}{\rho}\frac{\partial \overline{p}}{\partial x_i} + \nu \frac{\partial^2 \overline{u}_i}{\partial x_j \partial x_j}, \tag{3}$$

where the overline denotes the grid-filtering operator and $\tau_{ij} = \overline{u_i u_j} - \overline{u}_i \overline{u}_j$ is the SGS stress. All the SGS models tested in this paper are based on the eddy viscosity concept:

$$\tau_{ij} = -2\,\nu_t\,\overline{S}_{ij} + \frac{2}{3}\delta_{ij} k_{SGS}\ , \quad \overline{S}_{ij} = \frac{1}{2}\left(\frac{\partial \overline{u}_i}{\partial x_j} + \frac{\partial \overline{u}_j}{\partial x_i}\right). \tag{4}$$

Usually, the isotropic component, $(2/3)\,\delta_{ij} k_{SGS}$, is included in the pressure term. Namely, the pressure p in Eq. (3) is replaced by $p + (2/3)\,k_{SGS}$.

SUBGRID-SCALE MODELS

Smagorinsky Model

The widely used Smagorinsky model is as follows:

$$\nu_t = \left(Csf\overline{\Delta}\right)^2 |\overline{S}|\ , \quad |\overline{S}| = \sqrt{2\left(\overline{S}_{ij}\,\overline{S}_{ij}\right)}, \tag{5}$$

where $\overline{\Delta} = (\Delta x\,\Delta y\,\Delta z)^{1/3}$, and f is a wall-damping function.

Dynamic Smagorinsky Model

In the dynamic Smagorinsky Model, the test filter is applied to the grid-filtered flow field. The sub-test-scale stress

is defined as $T_{ij} = \widetilde{\overline{u_i u_j}} - \widetilde{\overline{u}}_i \widetilde{\overline{u}}_j$, where $\widetilde{(\ )}$ denotes the test-filtering operator. Using the "Germano identity," a stress tensor L_{ij} is defined as $L_{ij} = T_{ij} - \widetilde{\tau_{ij}} = \widetilde{\overline{u}_i \overline{u}_j} - \widetilde{\overline{u}}_i \widetilde{\overline{u}}_j$. By assuming the Smagorinsky model for both T_{ij} and τ_{ij}, the following relation is obtained: $L^*_{ij} = -2C\widetilde{\overline{\Delta}}^2 M_{ij}$, where $M_{ij} = \alpha^2 |\widetilde{\overline{S}}| \widetilde{\overline{S}}_{ij} - \widetilde{|\overline{S}| \overline{S}_{ij}}$, $C = (Cs\,f)^2$ and $\alpha = \widetilde{\overline{\Delta}} / \overline{\Delta}$. The parameter C is computed by applying a least-square approach as follows:

$$C = -\frac{1}{2} \frac{L^*_{ij} M_{ij}}{\overline{\Delta}^2 M_{ij} M_{ij}}. \tag{6}$$

Consequently, there is no need to give the model parameter or a wall-damping function beforehand. In this study, we set $\alpha = 2$. The ratio of the test filter width to the grid filter width, γ, is set to $\sqrt{3}$. We adopt the formula elaborated by Taniguchi (1995) for the test filtering operation so that the effects of the aliasing and truncation errors on the L_{ij} and M_{ij} are reduced.

Mixed-Time-Scale SGS Model

The mixed-time-scale SGS model (Inagaki *et al.* 2002a) obeys the following expression of the eddy viscosity: $\nu_t \propto$ (Velocity scale)^2 $\times$ (Time scale). The velocity scale is given by k_{es}, where k_{es} is the SGS turbulent energy estimated by filtering a velocity field (e.g., Horiuti, 1993):

$$k_{es} = \left(\overline{u}_k - \widehat{\overline{u}}_k\right)^2. \tag{7}$$

The notation, $\widehat{(\ )}$, denotes the filtering operator, for which the Simpson rule is adopted. This estimation procedure is based on a concept resembling that of scale similarity.

The time scale is defined as the harmonic average of two time scales. One is $\overline{\Delta} / \sqrt{k_{es}}$, which stands for the characteristic time scale of the small scales corresponding to the cut-off scale. The other is $1 / |\overline{S}|$, which stands for that of the large scales. It has been established that $1 / |\overline{S}|$ is a proper time scale near the wall and makes it possible to dispense with a wall-damping function. Consequently, the present model is described as follows:

$$\nu_t = C_{MTS}\, k_{es}\, T_s\,, \quad T_s^{-1} = \left(\frac{\overline{\Delta}}{\sqrt{k_{es}}}\right)^{-1} + \left(\frac{C_T}{|\overline{S}|}\right)^{-1}. \tag{8}$$

The model parameters C_{MTS} and C_T are set to 0.05 and 10, respectively.

NUMERICAL METHODS

We employ a second-order collocated grid system, which is modified from the original one (Rhie and Chow, 1983 or Morinishi *et al.*, 1998). The modification has two points. One is the interpolation method of the auxiliary flux velocity components U_i at the center of the cell faces. We use a fourth-order interpolation instead of a second-order one. The other is the discretization method for the pressure gradient at the center of the cells. We use a combination of three-fourths of a fourth-order central difference scheme and one-fourth of a second-order central difference scheme. Owing to this modification, the present grid system has almost the same numerical accuracy as the second-order staggered grid system, and is readily applicable to curvilinear grids. It should be noted that the Poisson equation for pressure is discretized in the same way as in the original collocated grid system using the auxiliary flux velocity components U_i. The stencil of the left-hand side of the Poisson equation is the same as in the original one, and thus the increase in computational cost using the present grid system is negligible. The convection terms are advanced explicitly using the second-order Adams-Bashforth method, whereas the viscous terms are advanced implicitly using the Crank-Nicolson method.

We use the cell-centered grid system, so that the wall-pressure, p_w, must be estimated in some way. Since the flows we focused on are high Reynolds number flows, the Neumann condition can be imposed for pressure. However, the pressure in the computation includes the isotropic component of the SGS stress, k_{SGS}. In the present study, k_{SGS} is estimated as $0.6k_{es}$, where the coefficient, 0.6, is decided by considering the following facts: (1) The model parameter of one-equation model is typically 0.7; (2) The optimized model parameter of a single-time-scale model ($\nu_t \approx f\overline{\Delta}\sqrt{k_{es}}$) in a channel flow is around 0.4. As a result, the wall-pressure is given as follows:

$$p_w = (p - 0.4k_{es})|_1\,, \tag{9}$$

where subscript 1 represents the nearest cell-center point to the wall.

RESULTS

Flow around a Circular Cylinder

The Aeolian tone generated by a circular cylinder is one of the most frequently encountered aerodynamic noises. In the present calculations, the Reynolds number based on the diameter of the circular cylinder and the mean inflow velocity, $Re = DU_0/\nu$, is set to 10,000. Figure 1 shows the computational domain. We employ the overlaid grid system (e.g., Horinouchi 1995) to reduce the computational cost. The computational domain is divided into two sub-domains. Sub-domain 1 surrounds the circular cylinder with a radial extent of about $1.7D$, while sub-domain 2 covers the whole computational domain. The number of grid points in sub-domain 1 is $160 \times 56 \times 20$, and $96 \times 60 \times 20$ in sub-domain 2. The minimum grid spacing is $4 \times 10^{-3}D$. The spanwise extent of the domain is set to $2D$, and the periodic condition is imposed to that direction. A no-slip boundary condition is applied on the wall, and a uniform flow condition is imposed at the inflow boundary. At the outflow boundary, the convective boundary condition is applied, where the convective velocity is set equal to the inflow velocity.

In the Smagorinsky model, Cs is set to 0.1 (S1 model) and 0.15 (S2 model). The former is the value used in the previously conducted test cases of channel flows and backward-facing step flow, while the latter is the value generally used in outer flow calculations. The wall-damping function is given as $f = \min\left(1, \sqrt{5n/D}\right)$, the validity of which in this flow field is ascertained by Kato & Ikegawa (1991). In the dynamic Smagorinsky (DS) model, the parameter C is calculated by taking the average over the spanwise direction and is set to zero at those locations where C is calculated to be negative. Additionally, we conduct a Q-DNS using QUICK scheme for the convection term, and also a LES using QUICK scheme together with the Smagorinsky model ($Cs = 0.15$). First, we compare the prediction accuracy of each method concerning the mean flow field and velocity fluctuations. Table 1 shows the calculated drag coefficient, C_D, root mean square of the lift coefficient fluctuation, C_{Lrms}, angle of the separation point, θ_{sp}, length of the recirculating region on the centerline, X_R,

Table 1: Results of flow around circular cylinder and time step.

	C_D	C_{Lrms}	θ_{sp}	X_R	St	Δt
Present	1.17	0.44	86 (deg)	0.83D	0.21	4×10^{-3}
S1 ($Cs = 0.1$)	1.32	0.61	86 (deg)	0.75D	0.21	4×10^{-3}
S2 ($Cs = 0.15$)	1.19	0.39	85 (deg)	0.95D	0.21	4×10^{-3}
DS	1.08	0.39	86 (deg)	0.91D	0.21	2×10^{-3}
QUICK	1.00	0.10	81 (deg)	1.80D	0.22	(4×10^{-3})
S2+QUICK	1.00	0.13	83 (deg)	1.62D	0.22	(4×10^{-3})
Exp.	1.1 – 1.2	0.3 – 0.5	—	≈1 D	0.20–0.21	—

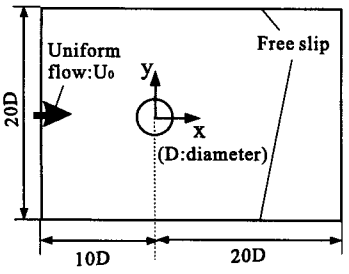

Figure 1: Flow around circular cylinder.

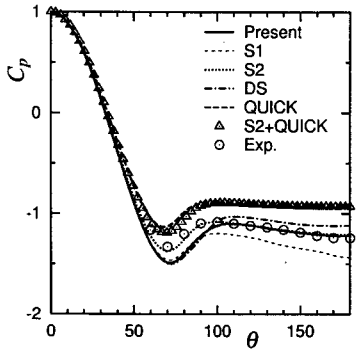

Figure 2: Pressure distribution on circular cylinder.

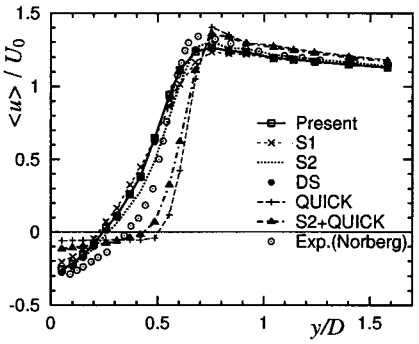

Figure 3: Mean streamwise velocity in x=1 plane.

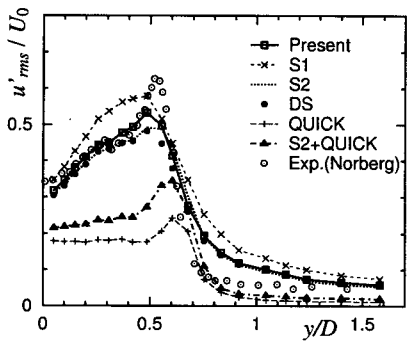

Figure 4: Streamwise velocity fluctuation in x=1 plane.

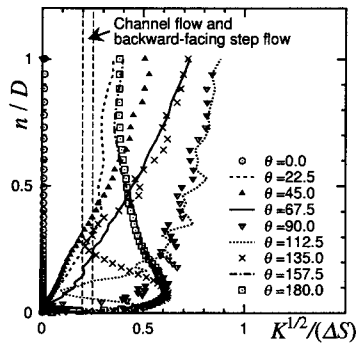

Figure 5: Ratio of two time scales used in the present model.

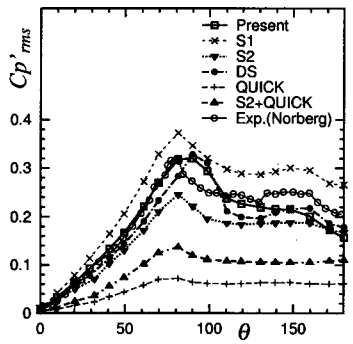

Figure 6: Pressure fluctuation on cylinder surface.

Strouhal number, St, and the dimensionless time step, Δt, allowing for a stable calculation. Figure 2 shows the distributions of pressure coefficients on the cylinder surface, and Figs. 3 – 4 show the results on the $x/D = 1.0$ line. The present model and S2 model predict the C_D to be in fair agreement with the experimental result, while the DS model shows less accuracy in pressure distribution on the cylinder surface (especially $\theta > 100°$) and less computational stability, similar to the previously reported test cases. The S1 model underpredicts the base pressure, while the present model predicts it accurately, although the same model parameters as in the previous test cases are used. Thus, the present model is considered to be more universal than the Smagorinsky model. Figure 5 shows the ratio of two time scales, $R = \sqrt{k_{es}} / \left(\overline{\Delta} S\right)$, used in the present model. Note that the present model can be rewritten as $\nu_t = C_{MTS} / \left\{1 + (RC_T)^{-1}\right\} \overline{\Delta}\sqrt{k_{es}}$. This means that the present model corresponds to a single-time-scale model, $\nu_t \approx \overline{\Delta}\sqrt{k_{es}}$, with the model parameter dependent on R. In the channel flows and backward-facing step flow (Inagaki *et al.* 2002a), R was 0.20 – 0.25, while it takes a higher value varying from 0.4 to 0.8 in the wake region of this flow field. If R rises from 0.225 to 0.6, ν_t increases by 24 %. This property may be one reason why the present model gives accurate results with the consistent model parameters. In the laminar flow region, since $\sqrt{k_{es}}$ approaches zero, ν_t given by the present model is found to become nearly zero, as in the DS model.

It is also demonstrated that Q-DNS (QUICK) has less accuracy than LES except when using the S1 model. Q-DNS overpredicts the base pressure, which leads to an underestimation of C_D. In addition, the X_R obtained by Q-DNS is much longer than the experimental data and LES results, which may be due to the weaker turbulence calculated in the separation region, as shown in Fig. 4. This inaccuracy in turbulent quantities is considered to be a consequence of the artificial viscosity introduced by the QUICK scheme. It should be noted that the LES calculation together with the QUICK scheme (S2+QUICK) gives similar results to those obtained by Q-DNS. This indicates that the artificial viscos-

ity introduced by a third-order upwind difference scheme has much stronger effects on turbulence than the SGS model. For that reason, in LES, a third-order upwind difference scheme for the convection term should not be adopted.

Second, the wall-pressure fluctuations, Cp'_{rms}, are compared in Fig. 6. The spectrum of those fluctuations has a strong peak (not shown here) which correlates with the Karman vortex shedding. The LES results using the present model are in best agreement with the experimental results, while the results of Q-DNS show less amplitude compared with those of LES and the experimental data. The lesser amplitude of wall-pressure fluctuation is consistent with the weaker turbulence mentioned above, and is probably also caused by the artificial viscosity. LES using QUICK scheme continues to give similar results to those of Q-DNS.

The C_{Lrms}, shown in Table 1 is a measure of the wall-pressure fluctuation and radiated sound noise. The value of C_{Lrms} obtained by Q-DNS or LES using QUICK scheme is about a third or a fourth of the experimental result, which corresponds to an underestimation of the radiated sound pressure level by around 10 dB. This inaccuracy is considered to be a significant problem in predicting aerodynamic noise.

Flow around a Simplified Front-Pillar Model

Wind noise from the front-pillar is one of the greatest problems associated with automobiles. To examine the validity of the present LES method, we apply it to the flow around a simplified front-pillar model as shown in Fig. 7. For comparison with the computations, the experiments are performed in the RTRI's low-noise wind tunnel with a 3×2.5 m open test section. The body height is 0.606 m. The incoming flow velocity is set to 27.8 m/s. The background noise level under those conditions is less than 45 dB. The pressure fluctuations are measured on the surface of the side window by pressure sensors.

The computational domain is divided into five sub-domains. For sub-domain 1 that surrounds the main part of the body, we use three different grid resolutions so as to examine the grid-dependency as shown in Table 2. The total number of grid points of other sub-domains is about 350,000. The artificial wall condition, which assumes the three-layer wall function modified from the two-layer one proposed by Werner & Wengle (1991), is applied at the wall surface. The wall coordinates at the center of the grid cells adjacent to the body surface vary approximately from 0.6 to 13 in the LES with the finest grid (Grid 3). As for LES, the dynamic Smagorinsky model does not maintain a stable computation even by setting the time step to one-forth of that in the calculation for the present model when using Grid 1. Therefore, all LES results shown in the following are those using the present model.

Figure 8 shows the comparison between the oilflow pattern in the experiment and the mean streamline near the wall predicted by LES with Grid 3. The L1 lines are the reattachment lines, while the L2 lines are the separation lines of the secondary vortices. It can be seen that the computation predicts these characteristic lines accurately. Figure 9 (b) shows the mean pressure coefficient obtained by each computation at the measuring points seen in Figure 9 (a). It is found that the LES with Grid 2 or Grid 3 provides results most close to the experimental data. The LES with Grid 1 reduces the accuracy at points 16 and 17. On the other hand, the Q-DNS with Grid 1 underpredicts the pressure coefficient at points 7 – 9. The Q-DNS with Grid 2 improves the accuracy at those points, while it predicts poorly at points 13 – 17.

Table 2: Grid point number of sub-domain 1 (Front-Pillar model).

Grid	Grid points	Grid point number on side window	Δy_{min}(m)
1	$99 \times 40 \times 174 = 689,040$	2,115	2×10^{-4}
2	$179 \times 51 \times 224 = 2,044,896$	5,700	1×10^{-4}
3	$246 \times 51 \times 324 = 4,064,904$	13,500	1×10^{-4}

Figure 10 shows the spectra of wall-pressure fluctuations near a reattachment point (see Fig. 8, point A). The experimental data demonstrate that the wall-pressure fluctuation has a wide-range spectrum. Although both LES and Q-DNS give insufficient results in the high-frequency range even when using the highest grid resolution (Grid 3), the results of LES show better agreement with the experimental data than those of Q-DNS in the high-frequency range. Using a lower grid resolution (Grid 1), the disagreement with the experimental data is seen from the lower frequency ranges in the results of both LES and Q-DNS. In Fig. 10, f_Δ is a roughly estimated frequency that is equivalent to the cut-off wave number on the assumption of frozen turbulence:

$$f_\Delta = \frac{U_c}{2\pi\overline{\Delta}_1}, \tag{10}$$

where U_c is set to half of the inflow velocity since the vortices generating in shear layers ordinarily convect with about half of the velocity difference of the shear flow, and $\overline{\Delta}_1$ is the filter width next to the wall. Theoretically, the computation cannot predict a higher frequency range than f_Δ. The estimated f_Δ for three grids almost corresponds to the frequencies where the results of LES begin to decline in comparison with the experimental data, so that it can be said that the present LES fully utilizes the given grid resolution. Note that LES with Grid 1 has the same level of predictability as the Q-DNS with Grid 2. The filter width of Grid 1, $\overline{\Delta}_{1Grid1}$ is about two times that of Grid 2, $\overline{\Delta}_{1Grid2}$. Thus, the Q-DNS may require approximately eight times as many grid points to achieve the same level of accuracy as in the present LES method. When using such a finer grid, the minimum grid spacing also restricts the computational time step. However, this may be compensated by the higher computational stability of Q-DNS than that of the present LES. For example, the computational time step in the Q-DNS with Grid 2 is 2×10^{-4}, while that in the LES is 1×10^{-4}. The increase of computational cost caused by calculating the modeled SGS stress term is about 30%. As a result, LES can be expected to reduce the computational cost by more than 80% in comparison with Q-DNS.

CONCLUSIONS

The high accuracy and high computational stability of the new mixed-time-scale SGS model have been confirmed in the calculation of the flow around a circular cylinder as well as in that of the channel flow and backward-facing step flow. The high accuracy arises from the introduction of the mixed time scale, while the high computational stability is

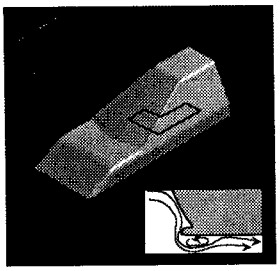

Figure 7: A simplified front-pillar model.

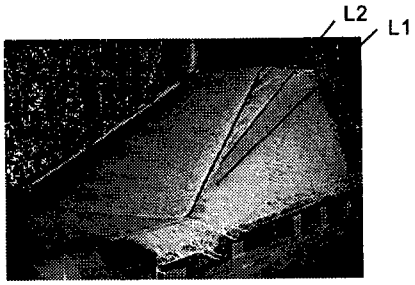

(a) Oilflow in experiment.

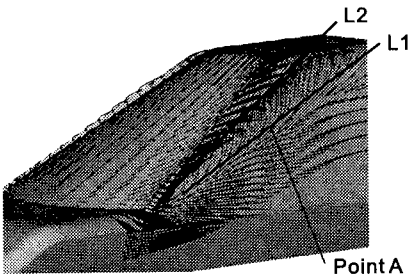

(b) Streamline near wall by LES (Grid 3).

Figure 8: Comparison of near-wall velocity distribution.

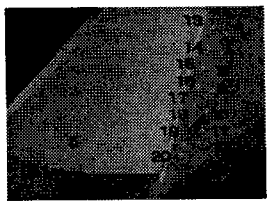

(a) Measuring points.

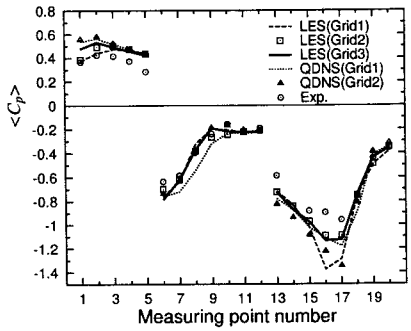

(b) Mean pressure coefficient.

Figure 9: Comparison of mean pressure coefficient on body surface.

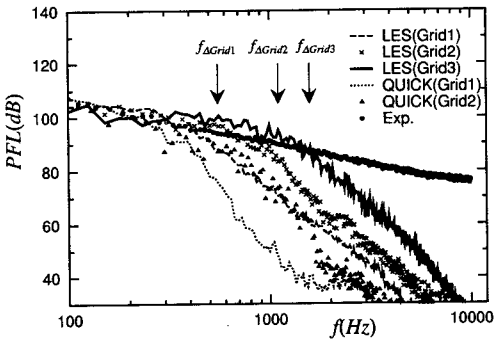

Figure 10: Comparison of spectrum of wall-pressure fluctuation (Point A).

due to the fixed-model parameters. The study has demonstrated that LES using the new model has a higher accuracy in predicting the wall-pressure fluctuations than Quasi-DNS. The superiority of the present LES is observed in the prediction both of the fluctuations with wide-range spectra and of those with a strong peak spectrum. Furthermore, it is apparent that the accuracy of LES employing a third-order upwind scheme is notably lower than LES employing a second-order central difference scheme, and is rather similar to that of Quasi-DNS. It can be concluded that the present LES method using the mixed-time-scale SGS model is effective for predicting certain kinds of wall-pressure fluctuations in practical applications.

REFERENCES

Curle, N., 1955, "The influence of solid boundaries upon aerodynamic sound," *Proc. R. Soc. London*, A231, pp. 481–484.

Germano, M., Piomelli, U., Moin, P. and Cabot, W. H., 1991, "A dynamic subgrid-scale eddy viscosity model", *Phys. Fluids*, A3, No. 7, pp. 1760–1765.

Horinouchi, N., Kato, Y., Shinano, S., Kondoh, T. and Tagayashi, Y., 1995, "Numerical investigation of vehicle aerodynamics with overlaid grid system," *SAE Paper* 950628.

Horiuti, K., 1993, "A proper velocity scale for modeling subgrid-scale eddy viscosities in large eddy simulation," *Phys. Fluids*, A5, No. 1, pp. 146–157.

Inagaki, M., Kondoh, T. and Nagano, Y., 2002a, "A mixed-time-scale SGS model with fixed model-parameters for practical LES", In *Engineering Turbulence Modelling and Experiments 5*, pp. 257–266, Elsevier.

Inagaki, M., Murata, O., Kondoh, T. and Abe, K., 2002b, "Numerical prediction of fluid-resonant oscillation at low Mach number", *AIAA Journal*, Vol. 40, pp. 1823–1829.

Jordan, S. A., 2002, "Investigation of the cylinder separated shear-layer physics by large-eddy simulation," *Int. J. Heat and Fluid Flow*, Vol. 23, pp. 1–12.

Kato, C. and Ikegawa, M., 1991, "Large eddy simulation of unsteady turbulent wake of a circular cylinder using the finite element method," ASME FED-Vol.117, Advances in Numerical Simulation of Turbulent Flows.

Mityata, M. and Okuyama, T., 1997, "Some methods for drag reduction of circular cylinder in uniform flow," *Proceedings of JSFM Symposium on Turbulent Flows* (in Japanese), pp. 147–148.

Morinishi, Y., Lund, T. S., Vasilyev, O. V. and Moin, P., 1998, "Fully conservative higher order finite difference schemes for incompressible flow," *J. Comput. Phys.*, Vol. 143, pp. 90–124.

Neto, A. S., Grand, D., Métais, O and Lesieur, M., 1993, "A numerical investigation of the coherent vortices in turbulence behind a backward-facing step," *J. Fluid Mech.*, Vol. 256, pp. 1–25.

Norberg, C., 1998, "LDV-measurements in the near wake of a circular cylinder," *ASME Fluids Engineering Division Summer Conference Paper* FEDSM98-5202.

Rhie, C. M. and Chow, W. L., 1983, "Numerical study of the turbulent flow past an airfoil with trailing edge separation," *AIAA Journal*, Vol. 21, pp. 1525–1532.

Taniguchi, N., 1995, "Dynamic SGS model by finite difference method," *Monthly Journal of Institute of Industrial Science (University of Tokyo)*, Vol. 47, No. 2, pp. 42–45.

Werner, H. and Wengle, H., 1991, "Large eddy simulation of turbulent flow over and around a cube in a plane channel," *Proceedings of 8th Symposium on Turbulent Shear Flows*, 19-4-1–19-4-6.